

# Extracting the glue-gluon distribution amplitude of the $\eta$ and $\eta'$ mesons

P. Kroll <sup>1</sup>

*Fachbereich Physik, Universität Wuppertal, D-42097 Wuppertal, Germany*  
and  
*Institut für Theoretische Physik, Universität Regensburg,  
D-93040 Regensburg, Germany*

K. Passek-Kumerički <sup>2</sup>

*Theoretical Physics Division, Rudjer Bošković Institute, Zagreb, Croatia*

## Abstract

The  $\eta\gamma$  and  $\eta'\gamma$  transition form factors are analyzed to leading-twist accuracy and next-to-leading order (NLO) of perturbative QCD. Using an  $\eta-\eta'$  mixing scheme and all currently available experimental data the lowest Gegenbauer coefficients of the distribution amplitudes for the valence octet and singlet  $q\bar{q}$  and the gluon-gluon Fock components are extracted. Predictions for the  $g^*g^*\eta'$  vertex function are presented. We also comment on the new BELLE results for the  $\pi\gamma$  transition form factor.

## 1 Introduction

The recent measurements of the photon to pseudoscalar meson transition form factors at large photon virtualities,  $Q^2$ , by the BaBar collaboration

---

<sup>1</sup>Email: kroll@physik.uni-wuppertal.de

<sup>2</sup>Email: passek@irb.hr

[1, 2] caused much excitement and renewed the interest in the theoretical description of these observables. Most surprising is the seemingly sharp rise of the  $\pi\gamma$  form factor with the photon virtuality, which is difficult to accommodate in fixed-order perturbative QCD. Power corrections to the usual leading-twist (collinear) approach [3] seem to be required. However, there is also a measurement of this form factor by the BELLE collaboration [4] which shed doubts on the BaBar data. At large  $Q^2$  the results of the two measurements differ, the BELLE results are close to the theoretical expectations from the leading-twist approach. Also the  $\eta\gamma$  and  $\eta'\gamma$  form factor data behave as expected according to theoretical analyses [5, 6, 7] of the CLEO [8] and L3 data [9], measured at lower  $Q^2$  than the BaBar data. Strong power corrections are not demanded in these analyses. Indeed a next-to-leading order (NLO) leading-twist analysis [6] is in reasonable agreement with the CLEO and L3 data. It is therefore tempting to reanalyze the  $\eta\gamma$  and  $\eta'\gamma$  form factors to this accuracy along the lines presented in [6], taking into account the new BaBar data. It should be mentioned that the combined CLEO, L3 and BaBar data on these two form factors have already been analyzed in other approaches. Thus, for instance, in [10]  $\mathbf{k}_\perp$  factorization is exploited or, in [11], light-front holographic QCD. In [12] the low  $Q^2$  data have been studied within the non-local chiral quark model and in [13] the dispersive representation of the axial anomaly is used to derive an expression for the form factors that holds at all  $Q^2$ . In [14] the anomaly sum rule has also been exploited for the analysis of the transition form factors. A combined analysis of the low and high  $Q^2$  data has also been performed in [15].

The  $\eta$  and  $\eta'$  mesons possess  $SU(3)_F$  singlet and octet quark-antiquark Fock components and, additionally, two-gluon ones leaving aside higher Fock states. Leading-twist distribution amplitudes,  $\phi$ , are associated with each of these Fock components. This feature leads, on the one hand, to the well-known flavor mixing and, on the other hand, as a further complication, to mixing of the  $q\bar{q}$  singlet and the gluon-gluon ( $gg$ ) distribution amplitudes under evolution. In the case of the transition form factors the two-gluon Fock components do not contribute to leading order (LO), they require higher orders of perturbative QCD. In our previous analysis [6] of the  $\eta\gamma$  and  $\eta'\gamma$  transition form factors to NLO leading-twist accuracy (see Fig. 1 for relevant Feynman graphs) the short lever arm provided by the  $Q^2$  range of the CLEO and L3 data, the overall number of the data as well as the size of their errors, made it impossible to fix precisely even the lowest Gegenbauer coefficients of the distribution amplitudes. The resulting values were subject to substantial

errors. In particular we didn't find a clear signal for the  $gg$  distribution amplitudes, a zero effect could not be excluded. Here, in this work we attempt a reanalysis of the form factors, using in addition to the CLEO and L3 data also the recent BaBar data [2]. With our analysis we want to demonstrate that, in contrast to the case of the pion, the  $\eta$  and  $\eta'\gamma$  form factor data can easily be accommodated by a QCD calculation to NLO leading-twist accuracy. A second goal of our analysis is the determination of the  $gg$  distribution amplitudes. On the strength of a larger set of data covering a substantially larger range of  $Q^2$ , more precise results for the gluon distribution amplitudes than obtained in [6] can be expected and indeed, as it will turn out, is found. This is of utmost importance since the two-gluon Fock components play a role in many hard exclusive processes involving  $\eta$  and/or  $\eta'$  mesons which are nowadays accessible to experiment. Thus, for instance, the  $g^*g^*\eta(\eta')$  vertex contributes to decay processes such as  $\Upsilon(1S) \rightarrow \eta'X$  (see e.g. [16, 17]), to the hadronic production  $pp(\bar{p}) \rightarrow \eta'X$  and to meson pair production in the central region of proton-proton collisions [18]. The two-gluon Fock components may also matter in  $\chi_{cJ}$  decays in pairs of  $\eta$  or  $\eta'$  mesons and they may be attributed to the enhancement of some of the  $\eta'$  channels in charmless  $B$  decays as compared to the corresponding pion channels (e.g. [19, 20, 21]). An example is set by the  $\eta'K$  channels for which such an enhancement is experimentally observed [22, 23]. In this context the  $B \rightarrow \eta(\eta')$  form factors are of importance which are also affected by the  $gg$  component of the  $\eta$  and  $\eta'$  mesons (e.g. [24]).

The plan of the paper is the following: In Sect. 2 we recapitulate properties of the  $q\bar{q}$  and  $gg$  distribution amplitudes for the  $\eta$  and  $\eta'$  mesons, in particular their evolution behavior. The transition form factors to NLO leading-twist accuracy are presented in Sect. 3 while, in the next section,  $\eta - \eta'$  mixing is briefly discussed. The CLEO [8] and BaBar [2] data on the transition form factors are analyzed for several scenarios in Sect. 5 and values for the second Gegenbauer coefficients of the three distribution amplitudes are extracted. We also shortly comment on the data for the time-like transition form factors obtained by BaBar [25]. Implications of the resulting distribution amplitudes for the  $g^*g^*P$  vertex are discussed in Sect. 6 and a brief comment on the  $\pi\gamma$  transition form factor is given in Sect. 7. As usual the paper ends with a summary.

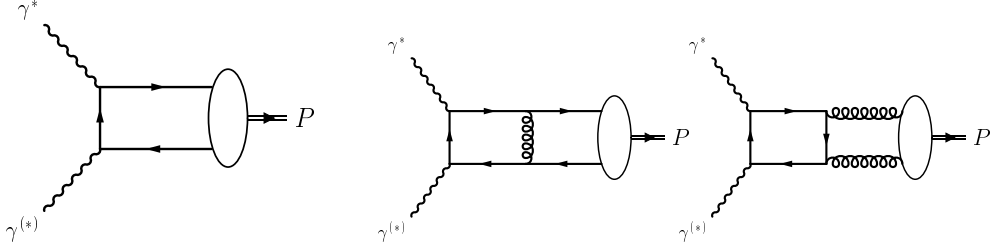


Figure 1: Sample Feynman graphs contribution to the transition form factors to NLO.

## 2 Properties of the distribution amplitudes

When considering the evolution and mixing of quark and gluon states under evolution, it is convenient to choose  $SU(3)_F$  octet and singlet combinations of quark-antiquark states [6] as valence Fock components of the pseudoscalar mesons,

$$\begin{aligned} |q\bar{q}_8\rangle &= |(u\bar{u} + d\bar{d} - 2s\bar{s})/\sqrt{6}\rangle \\ |q\bar{q}_1\rangle &= |(u\bar{u} + d\bar{d} + s\bar{s})/\sqrt{3}\rangle \end{aligned} \quad (1)$$

and the two-gluon state,  $|gg\rangle$ , which also possess flavor-singlet quantum numbers and contributes to leading-twist order. Higher Fock components are neglected in our analysis since their contributions are power suppressed. It is to be stressed that the above states are partonic Fock components and not effective meson states or glueballs which are frequently considered in the treatment of  $\eta - \eta'$  mixing. In collinear approximation and to leading-twist accuracy a distribution amplitude,  $\phi_{P_i}$ , is associated with each of the Fock components we consider<sup>3</sup>. They satisfy the symmetry relations ( $i = 1, 8, P = \eta, \eta'$ )

$$\phi_{P_i}(x, \mu_F) = \phi_{P_i}(1 - x, \mu_F), \quad \phi_{P_g}(x, \mu_F) = -\phi_{P_g}(1 - x, \mu_F). \quad (2)$$

The quark distribution amplitudes are normalized to unity at any factorization scale  $\mu_F$

$$\int_0^1 dx \phi_{P_i}(x, \mu_F) = 1 \quad (3)$$

<sup>3</sup>A formal definition of the leading-twist distribution amplitudes in terms of particle-vacuum matrix elements of quark field operators or the gluon field strength tensor can be found in [6].

while for the gluon distribution amplitude one has

$$\int_0^1 dx \phi_{Pg}(x, \mu_F) = 0. \quad (4)$$

Thus, there is no natural way to normalize the latter distribution amplitude, but its mixing with the quark distribution amplitude under evolution removes this ambiguity and, as shown in [6], the change in gluon normalization is reflected in the change of off-diagonal anomalous dimensions governing the evolution – for details, see below.

The distribution amplitudes can be expanded upon the Gegenbauer polynomials

$$\begin{aligned} \phi_{Pi}(x, \mu_F) &= 6x(1-x) \left[ 1 + \sum_{n=2,4,\dots} a_{Pn}^i(\mu_F) C_n^{3/2}(2x-1) \right], \\ \phi_{Pg}(x, \mu_F) &= x^2(1-x)^2 \sum_{n=2,4,\dots} a_{Pn}^g(\mu_F) C_{n-1}^{5/2}(2x-1), \end{aligned} \quad (5)$$

where only the terms for even  $n$  occur as a consequence of the symmetry relations (2). In terms of the expansion coefficients  $a_{Pn}$  the mixing of the quark singlet and gluon distribution amplitudes are expressed by

$$\begin{aligned} a_{Pn}^1(\mu_F) &= a_{Pn}^{(+)}(\mu_0) \left( \frac{\alpha_s(\mu_0)}{\alpha_s(\mu_F)} \right)^{\gamma_n^{(+)}/\beta_0} + \rho_n^{(-)} a_{Pn}^{(-)}(\mu_0) \left( \frac{\alpha_s(\mu_0)}{\alpha_s(\mu_F)} \right)^{\gamma_n^{(-)}/\beta_0}, \\ a_{Pn}^g(\mu_F) &= \rho_n^{(+)} a_{Pn}^{(+)}(\mu_0) \left( \frac{\alpha_s(\mu_0)}{\alpha_s(\mu_F)} \right)^{\gamma_n^{(+)}/\beta_0} + a_{Pn}^{(-)}(\mu_0) \left( \frac{\alpha_s(\mu_0)}{\alpha_s(\mu_F)} \right)^{\gamma_n^{(-)}/\beta_0}, \end{aligned} \quad (6)$$

where  $\mu_0$  is the initial scale of the evolution and  $\beta_0 = 11/3N_c - 2/3n_f$ . The number of colors is denoted by  $N_c$  and  $n_f$  is the number of active flavors at the characteristic scale of the process. The coefficients of the eigenfunctions of the matrix evolution equation which introduces mixing between quark and gluon distribution amplitudes, are here denoted by  $a_{Pn}^{(\pm)}$ . The powers  $\gamma_n^{(\pm)}$  are the eigenvalues of the matrix of anomalous dimensions [26, 27]

$$\gamma_n^{(\pm)} = \frac{1}{2} \left[ \gamma_n^{qq} + \gamma_n^{gg} \pm \sqrt{(\gamma_n^{qq} - \gamma_n^{gg})^2 + 4\gamma_n^{qg}\gamma_n^{gq}} \right], \quad (7)$$

where the LO elements of that matrix read ( $C_F = (N_c^2 - 1)/(2N_c)$ )

$$\gamma_n^{qq} = C_F \left[ 3 + \frac{2}{(n+1)(n+2)} - 4 \sum_{i=1}^{n+1} \frac{1}{i} \right],$$

$$\begin{aligned}
\gamma_n^{gg} &= C_F \frac{n(n+3)}{3(n+1)(n+2)} \quad n \geq 2, \\
\gamma_n^{gq} &= N_f \frac{12}{(n+1)(n+2)} \quad n \geq 2, \\
\gamma_n^{gg} &= \beta_0 + N_c \left[ \frac{8}{(n+1)(n+2)} - 4 \sum_{i=1}^{n+1} \frac{1}{i} \right] \quad n \geq 2. \quad (8)
\end{aligned}$$

It is helpful for the understanding of the following to introduce the distinction between the quantity  $N_f$  ( $= 3$ ) which counts the (fixed valence) quark content of the meson's flavor-singlet combination and the above defined  $n_f$ , the number of active flavors at some scale, which appears in the  $\beta$  functions and, as such, is connected to the running of the coupling constant. The parameters  $\rho_n^{(\pm)}$  in (6) read

$$\rho_n^{(+)} = 6 \frac{\gamma_n^{gq}}{\gamma_n^{(+)} - \gamma_n^{gg}}, \quad \rho_n^{(-)} = \frac{1}{6} \frac{\gamma_n^{gq}}{\gamma_n^{(-)} - \gamma_n^{gq}}. \quad (9)$$

The evolution of the octet distribution amplitude is merely governed by  $\gamma_n^{gq}$  and takes the simple form

$$a_{P_n}^8(\mu_F) = a_{P_n}^{(8)}(\mu_0) \left( \frac{\alpha_s(\mu_0)}{\alpha_s(\mu_F)} \right)^{\gamma_n^{gq}/\beta_0}. \quad (10)$$

To the order we are working, NLO evolution of the quark distribution amplitude should in principle be included. To this accuracy the Gegenbauer polynomials  $C_n^{3/2}$  are no longer eigenfunctions of the evolution kernel, i.e. their coefficients  $a_{P_n}^i$  do not evolve independently [28]. The impact of the NLO evolution on the transition form factors is expected to be small compared with the NLO corrections to the subprocess amplitudes [29]. Therefore we refrain from considering NLO evolution here.

The projection of a collinear  $q\bar{q}$  state onto a pseudoscalar state is achieved by replacing the quark and antiquark spinors by [30]

$$\mathcal{P}_{\alpha\beta,rs,kl}^i = \mathcal{C}_{i,rs} \frac{\delta_{kl}}{\sqrt{N_c}} \left( \frac{\gamma_5 \not{p}}{\sqrt{2}} \right)_{\alpha\beta}, \quad (11)$$

where  $p$  denotes the meson momentum, while  $\alpha$  ( $r, k$ ) and  $\beta$  ( $s, l$ ) represent Dirac (flavor, color) labels of the quark and antiquark, respectively. The

flavor matrices read

$$\mathcal{C}_8 = \frac{1}{\sqrt{2}}\lambda_8, \quad \mathcal{C}_1 = \frac{1}{\sqrt{N_f}}\mathbf{1}_f, \quad (12)$$

where  $\lambda_8$  is one of the usual  $SU(3)_F$  Gell-Mann matrices and  $\mathbf{1}_f$  is the  $3 \times 3$  unit matrix. The projector of a state of two (incoming) collinear gluons of color  $a$  and  $b$  and Lorentz labels  $\mu$  and  $\nu$  carrying the respective momentum fractions  $x$  and  $1 - x$  onto a pseudoscalar meson reads [6]

$$\mathcal{P}_{\mu\nu,ab}^g = \frac{i}{2} \sqrt{\frac{C_F}{N_f}} \frac{\delta_{ab}}{\sqrt{N_c^2 - 1}} \frac{\varepsilon_{\perp\mu\nu}}{x(1-x)}, \quad (13)$$

where

$$\varepsilon_{\perp}^{\mu\nu} = \varepsilon^{\mu\nu\alpha\beta} \frac{n_\alpha p_\beta}{n \cdot p} \quad (14)$$

( $\epsilon_{0123} = 1$ ) describes the helicity-zero combination of the two transverse gluon polarization vectors. Taking for the meson momentum  $p = [p^+, 0, 0_\perp]$ ,  $n$  in (14) is a light-like vector,  $n = [0, 1, 0_\perp]$ , which defines the plus component of a vector<sup>4</sup>,  $v^+ = n \cdot v$ . The factor  $[x(1-x)]^{-1}$  appearing in the projector (13), is a consequence of the conversion of the potential of the gluon field occurring in a perturbative calculation of reactions involving two-gluon Fock components, into the gluon-field-strength operator whose vacuum-meson matrix elements define the gluon distribution amplitude, see [31]. The projectors are to be used in calculations of hard partonic amplitudes which are to be convoluted with either  $f_P^i/(2\sqrt{2N_c})\phi_{Pi}$  or, for the gluons,  $f_P^1/(2\sqrt{2N_c})\phi_{Pg}$ . The decay constants,  $f_P^i$ , are, as usual, defined by vacuum-meson matrix elements of flavor singlet or octet weak axial-vector currents

$$\langle 0 | J_{\mu 5}^i(0) | P(p) \rangle = i f_P^i p_\mu. \quad (15)$$

The singlet decay constants,  $f_P^1$ , depend on the scale but the anomalous dimension controlling it is of order  $\alpha_s^2$  [32]. In fact the evolution of  $f_{P1}$  is part of the NLO evolution of the singlet distribution amplitude, it represents the scale dependence of its first Gegenbauer coefficient. This is to be contrasted to the octet distribution amplitude for which the first Gegenbauer coefficient,

---

<sup>4</sup>Actually, in (14) instead of  $n$  any four vector can be used that has a non-zero minus and a vanishing transverse component.

$a_0$ , is 1 at all scales. Thus, in harmony with the neglect of NLO evolution of the distribution amplitudes, the scale dependence of  $f_{P_1}$  is neglected too.

Finally, we comment on different conventions of gluon distribution amplitude and singlet evolution to be found in literature. A detailed comparison is given in [6]. There are two important observations. First, as explained in detail in [6], a change of the definition of the gluon distribution amplitude

$$\phi_{Pg}^\sigma = \sigma \phi_{Pg}. \quad (16)$$

is (due to the fact that the physical quantity is independent of the choice of the convention) accompanied by a corresponding change in the hard scattering amplitude, i.e., in the projector of  $gg$  state,  $\mathcal{P}_{\mu\nu}^{g\sigma} = 1/\sigma \mathcal{P}_{\mu\nu}^g$ , and (since the quark and gluon distribution amplitudes are connected through evolution) by a change of the off-diagonal anomalous dimensions

$$\gamma_n^{gg,\sigma} = \frac{1}{\sigma} \gamma_n^{gg}, \quad \gamma_n^{gq,\sigma} = \sigma \gamma_n^{gq}, \quad (17)$$

or, equivalently, the evolution kernels  $V_{gg}$  and  $V_{gq}$ . The analogous relations hold for any change in the definition of the quark distribution amplitude, but since in contrast to the gluon distribution amplitude, its normalization is well defined, the unique definition of the quark distribution amplitude is encountered throughout the literature.

Second, for historical reasons (see early work [27]) anomalous dimensions are in this field defined as in App. C of [6]:

$$V_{AB}(u, v) \otimes [\text{weight}_B](v) C^B(2v - 1) = \gamma_n^{AB} [\text{weight}_A](u) C^A(2u - 1), \quad (18)$$

where  $A, B \in \{q, g\}$  with corresponding notation  $C^q \equiv C_n^{3/2}$  and  $C^g \equiv C_{n-1}^{5/2}$  while  $[\text{weight}_q](u) = u(1 - u)$  and  $[\text{weight}_g](u) = u^2(1 - u)^2$ . On the other hand, the anomalous dimensions of the forward and non-forward parton distributions (appearing in deeply inelastic scattering and deeply virtual Compton scattering which are through operator product expansion closely connected to the meson transition form factors) are usually [33] defined as <sup>5</sup>

$$C^A(2u - 1) \otimes V_{AB}(u, v) = -^{AB} \gamma_n C^B(2v - 1). \quad (19)$$

---

<sup>5</sup>The additional factor 1/2 present in [33] is compensated by factor 2 in their definition for the evolution kernel.

This definition leads to

$${}^{qg}\gamma_n = \gamma_n^{qg} \frac{36}{n(n+3)}, \quad {}^{gq}\gamma_n = \gamma_n^{gq} \frac{n(n+3)}{36}. \quad (20)$$

Note that, as given in App. C of [6],

$$\frac{\gamma_n^{qg}}{\gamma_n^{gq}} = \frac{n(n+3)}{36}. \quad (21)$$

Thus in this case the difference in off-diagonal anomalous dimensions is not due to different definition of gluon distribution amplitude but rather to different defining equations of anomalous dimensions. When this, i.e., (20), is taken into account, one sees that our expressions are in agreement with [33], i.e., with the conventions used in deeply virtual processes.

### 3 The transition form factors

The  $\eta\gamma$  and  $\eta'\gamma$  transition form factors can be represented as a sum of flavor-octet and singlet contributions

$$F_{P\gamma}(Q^2) = F_{P\gamma}^8(Q^2) + F_{P\gamma}^1(Q^2), \quad (22)$$

where the singlet one also includes the gluon part. This decomposition is completely general. To NLO leading-twist accuracy the octet and singlet contributions can be written as [6]

$$\begin{aligned} F_{P\gamma}^8(Q^2) &= 2f_P^8 C_8 \int_0^1 dx \phi_{P8}(x, \mu_F) \frac{1}{xQ^2} \left[ 1 + \frac{\alpha_s(\mu_R)}{4\pi} C_F \mathcal{K}_q(x, Q^2, \mu_F) \right], \\ F_{P\gamma}^1(Q^2) &= 2f_P^1 C_1 \left\{ \int_0^1 dx \phi_{P1}(x, \mu_F) \frac{1}{xQ^2} \left[ 1 + \frac{\alpha_s(\mu_R)}{4\pi} C_F \mathcal{K}_q(x, Q^2, \mu_F) \right] \right. \\ &\quad \left. + \frac{\alpha_s(\mu_R)}{4\pi} C_F \int_0^1 dx \phi_{Pg}(x, \mu_F) \frac{2}{(1-x)^2 Q^2} \mathcal{K}_g(x, Q^2, \mu_F) \right\}. \end{aligned} \quad (23)$$

The meson and quark masses are neglected throughout. The  $\alpha_s$  correction to the quark parts, calculated in the  $\overline{MS}$  scheme [34, 35], read

$$\mathcal{K}_q(x, Q^2, \mu_F) = \ln^2 x - \frac{x \ln x}{1-x} - 9 - (3 + 2 \ln x) \ln \frac{\mu_F^2}{Q^2}, \quad (24)$$

while for the gluon contribution one has [6]

$$\mathcal{K}_g(x, Q^2, \mu_F) = -\frac{1}{2} \ln^2 x - \frac{1-3x}{x} \ln x + \ln x \ln \frac{\mu_F^2}{Q^2}. \quad (25)$$

The charge factors in (23) are

$$C_8 = \frac{e_u^2 + e_d^2 - 2e_s^2}{\sqrt{6}}, \quad C_1 = \frac{e_u^2 + e_d^2 + e_s^2}{\sqrt{N_f}}. \quad (26)$$

The charge of quark  $a$  in units of the positron charge is denoted by  $e_a$ . The  $x \leftrightarrow 1-x$  symmetry (2) of the distribution amplitudes has already been exploited in (23). As is well-known and can be seen from (5) – (8), the quark distribution amplitudes evolve into the asymptotic form

$$\phi_{AS} = 6x(1-x) \quad (27)$$

and the gluon one to zero for  $Q^2 \rightarrow \infty$ . In this limit the transition form factors become

$$F_{P\gamma} \rightarrow \sqrt{\frac{2}{3}} \frac{f_P^8 + 2\sqrt{2}f_P^1}{Q^2} \quad (28)$$

independently of the choice of the factorization scale.

In our analysis we do not take into account power corrections as for instance may arise from higher-twist effects <sup>6</sup>, from meson masses or from quark transverse degrees of freedom. The latter seem to be rather small for the form factors of interest, in fact much smaller than for the  $\pi\gamma$  transition form factor as is shown for instance in [10]. For further comments concerning power corrections see Sect. 5.

## 4 $\eta - \eta'$ mixing

In order to reduce the number of independent distribution amplitudes we follow [37] and assume meson independence of the distribution amplitudes, i.e.

$$\phi_{Pi} = \phi_i, \quad \phi_{Pg} = \phi_g \quad (29)$$

---

<sup>6</sup>It can be shown that there is no twist-3 correction to the transition form factor. Possible twist-4 and twist-6 corrections have been discussed for the case of the  $\pi\gamma$  form factor recently [36].

as we did in [6]. Hence, the mixing behavior of the valence Fock components and the particle dependence solely resides in the decay constants. Since in hard processes only small spatial quark-antiquark separations are probed, this assumption is sufficiently plausible - the decay constants play the role of wave functions at the origin of configuration space.

For the decay constants we use the general parametrization [32, 37]

$$\begin{aligned} f_\eta^8 &= f_8 \cos \theta_8, & f_\eta^1 &= -f_1 \sin \theta_1, \\ f_{\eta'}^8 &= f_8 \sin \theta_8, & f_{\eta'}^1 &= f_1 \cos \theta_1. \end{aligned} \quad (30)$$

In [37, 38] it has been observed that  $\eta - \eta'$  mixing is particularly simple in the quark-flavor basis defined by the transform

$$\begin{aligned} |\eta_q\rangle &= \cos \varphi |\eta\rangle + \sin \varphi |\eta'\rangle, \\ |\eta_s\rangle &= -\sin \varphi |\eta\rangle + \cos \varphi |\eta'\rangle, \end{aligned} \quad (31)$$

of the physical meson states. In this basis which is supposed to separate strange and non-strange contributions, the mixing behavior of the decay constants is controlled by the angles  $\varphi_q$  and  $\varphi_s$ , defined analogously to (30). It turned out from phenomenology that these angles practically fall together with the state mixing angle  $\varphi$ , i.e. that we can write

$$\begin{aligned} f_\eta^q &= f_q \cos \varphi, & f_\eta^s &= -f_s \sin \varphi, \\ f_{\eta'}^q &= f_q \sin \varphi, & f_{\eta'}^s &= f_s \cos \varphi. \end{aligned} \quad (32)$$

This observation is supported by a QCD sum rule study [39]. A recent lattice QCD study [40] is also not in conflict with it. The occurrence of only one mixing angle in this basis is a consequence of the smallness of OZI rule violations which amount to only a few percent and can safely be neglected in most cases.  $SU(3)_F$  symmetry, on the other hand, is broken at the level of 10 – 20%. The assumption  $\varphi_q = \varphi = \varphi_s$  is essential for the quark-flavor mixing scheme.

Working in the quark-flavor basis and exploiting the divergences of the axial-vector currents - which embody the axial-vector anomaly - the mixing parameters in the quark-flavor mixing scheme can be expressed in terms of the masses of the physical mesons [41], e.g.

$$\sin \varphi = \sqrt{\frac{(M_{\eta'}^2 - 2M_{K^0}^2 + M_{\pi^0}^2)(M_\eta^2 - M_{\pi^0}^2)}{2(M_{\eta'}^2 - M_\eta^2)(M_{K^0}^2 - M_{\pi^0}^2)}}. \quad (33)$$

	Ref.	$f_8/f_\pi$	$\theta_8$	$f_1/f_\pi$	$\theta_1$	$\varphi$
1	[41]	1.19	$-19.4^\circ$	1.10	$-6.8^\circ$	$41.4^\circ$
2	[37, 38]	1.26	$-21.2^\circ$	1.17	$-9.2^\circ$	$39.3^\circ$
3	[42]	1.51	$-23.8^\circ$	1.29	$-2.4^\circ$	$40.7^\circ$

Table 1: Decay constants in the singlet-octet basis and the mixing angle in the quark-flavor basis. The value of  $\varphi$  quoted in the last line for is the average of  $\varphi_q$  and  $\varphi_s$  determined in [42].

Evaluation of the mixing angle provides  $\varphi = 41.4^\circ$ . Using for the decay constant  $f_q$  in the quark-flavor basis the  $SU(3)_F$  symmetry result  $f_q = f_\pi$ , one finds for the strange decay constant in that basis

$$f_s = f_\pi \sqrt{\frac{(M_{\eta'}^2 - M_{\pi^0}^2)(M_\eta^2 - M_{\pi^0}^2)}{2(M_{\eta'}^2 - 2M_{K^0}^2 + M_{\pi^0}^2)(2M_{K^0}^2 - M_{\pi^0}^2 - M_\eta^2)}}. \quad (34)$$

Transforming these results to the octet-singlet basis, one obtains the results for the mixing parameters (30) that are quoted in Tab. 1. We repeat it is convenient to work in the latter basis because in it evolution which is an important ingredient to our analysis, is simple. In [37, 38] the mixing parameters have been determined phenomenologically using  $\varphi_q = \varphi = \varphi_s$  but allowing for higher-orders flavor symmetry breaking effects. The results, obtained from the analysis of a number of processes involving  $\eta$  and  $\eta'$  mesons, are also quoted in Tab. 1. For a discussion of uncertainties see [37]. There are a few more analyses, e.g. [39, 42, 43, 44], in which the decay constants (30) have been determined. In general the results are close to those obtained in [37, 38], for a comparison see [41]. The largest deviations from the mixing parameters given in [37, 38] has been reported in [42], see Tab. 1. This phenomenological analysis has been performed along the lines described in [37, 38] considering however only a subset of the processes investigated therein but, if at disposal, exploiting more recent data. In other papers only the mixing angle  $\varphi$  has been determined, e.g. [45, 46]. Within occasionally large errors the values for it ( $39 - 42^\circ$ ) agree with the ones found in [37, 38].

Frequently, mixing of the  $\eta$  and  $\eta'$  is studied starting from three basis states,  $\eta_8, \eta_1$  ( or  $\eta_q, \eta_s$ ) and a gluonic state  $\eta_g$ . Despite this the values for the

angle  $\varphi$  controlling  $\eta$ - $\eta'$  mixing obtained in such analyses agree reasonably well with the above quoted ones. However, these mixing schemes rely on the existence of a rather light pseudoscalar glueball for which there is no evidence, see the review [47]. In any case, it would be a misinterpretation to identify the gluon-gluon state we consider here with the  $\eta_g$ . Our gluon-gluon state is a partonic Fock component of the  $\eta$  and  $\eta'$ .

## 5 Analysis of the form factor data

Let us now turn to the extraction of the various distribution amplitudes or rather their Gegenbauer coefficients from the data on the transition form factors [2, 8, 9]. Inserting the Gegenbauer expansion of the distribution amplitudes (5) into (23) one can perform the integration term by term analytically. The result is

$$\begin{aligned}
Q^2 F_{P\gamma} &= a_{P0}^{\text{eff}}(\mu_F) \left[ 1 - \frac{5}{3} \frac{\alpha_s(\mu_R)}{\pi} \right] \\
&+ a_{P2}^{\text{eff}}(\mu_F) \left[ 1 + \frac{5}{3} \frac{\alpha_s(\mu_R)}{\pi} \left( \frac{59}{72} - \frac{5}{6} \ln \frac{Q^2}{\mu_F^2} \right) \right] \\
&+ a_{P4}^{\text{eff}}(\mu_F) \left[ 1 + \frac{5}{3} \frac{\alpha_s(\mu_R)}{\pi} \left( \frac{10487}{4500} - \frac{91}{75} \ln \frac{Q^2}{\mu_F^2} \right) \right] \\
&- \frac{20}{3\sqrt{3}} \frac{\alpha_s(\mu_R)}{\pi} f_P^1 \left[ a_2^g(\mu_F) \left( \frac{55}{1296} - \frac{1}{108} \ln \frac{Q^2}{\mu_F^2} \right) \right. \\
&\quad \left. + a_4^g(\mu_F) \left( \frac{581}{10125} - \frac{7}{675} \ln \frac{Q^2}{\mu_F^2} \right) \right] + \dots \quad (35)
\end{aligned}$$

where we introduced the abbreviation ( $n = 0, 2, 4, \dots$ ,  $a_0^i = 1$ )

$$a_{Pn}^{\text{eff}}(\mu_F) = \sqrt{\frac{2}{3}} \left[ f_P^8 a_n^8(\mu_F) + 2\sqrt{2} f_P^1 a_n^1(\mu_F) \right]. \quad (36)$$

Before we analyze the data a comment is in order: Inspection of (35) reveals the familiar result that only due the admittedly mild logarithmic  $Q^2$  dependence generated by the evolution and the NLO corrections one can in principle discriminate among the Gegenbauer coefficients of different orders. However, even with the large range of  $Q^2$  in which form factor data are available now, this logarithmic  $Q^2$  dependence is in practice insufficient to

Remarks	$\chi^2$	$a_2^8$	$a_2^1$	$a_2^g$	(41)
default	37.7	$-0.05 \pm 0.02$	$-0.12 \pm 0.01$	$19 \pm 5$	0.03
just [8]	18.5	$-0.07 \pm 0.03$	$-0.11 \pm 0.03$	$17 \pm 11$	0.02
just [2]	15.1	$-0.05 \pm 0.02$	$-0.12 \pm 0.01$	$33 \pm 9$	0.03
$\mu_R^2 = Q^2/2$	36.9	$-0.01 \pm 0.02$	$-0.08 \pm 0.01$	$10 \pm 4$	0.03
$\mu_R^2 = \mu_F^2 = Q^2/2$	37.5	$-0.01 \pm 0.02$	$-0.07 \pm 0.01$	$6 \pm 3$	0.03
mixing [42]	45.0	$0.05 \pm 0.02$	$-0.16 \pm 0.01$	$11 \pm 5$	0.10
$a_2^1 = a_8^1$	49.8	$-0.11 \pm 0.01$	$-0.11 \pm 0.01$	$21 \pm 5$	0.0
$a_2^1 = a_8^1$ , mix. [42]	240	$-0.16 \pm 0.01$	$-0.16 \pm 0.01$	$19 \pm 4$	0.0

Table 2: Gegenbauer coefficients at  $\mu_0 = 1$  GeV fitted to the data from [2] and [8] for  $Q^2 \geq 2$  GeV<sup>2</sup> (22 and 18 data points, respectively). Except stated otherwise, the standard setting described in the text (with  $\mu_F = \mu_R = Q$ ), and the mixing parameters of [37] are used (see Tab. 1). Eq. (41) is probed at  $\mu_0 = 1$  GeV.

allow for an extraction of more than one Gegenbauer coefficient for each of the distribution amplitudes [48]. In view of this problem, we are forced to truncate the Gegenbauer series at  $n = 2$ . To leading-twist accuracy the higher Gegenbauer coefficients are not suppressed as is the case for other approaches in which power corrections, accumulated in the soft end-point regions  $x \rightarrow 0$  or 1, are taken into account [10, 36]. Therefore the  $n = 2$  coefficients we are going to determine below, suffer from a truncation error; they are to be viewed as effective parameters which are contaminated by higher order Gegenbauer coefficients.

## 5.1 Fits

Except stated otherwise we employ the following specifications in our fits: As the minimum value of  $Q^2$  used in the fits we take 2 GeV<sup>2</sup> and for the initial scale of the evolution we choose  $\mu_0 = 1$  GeV. For  $\alpha_s$  we use the two-loop expression with four flavors ( $n_f = 4$ ) and  $\Lambda_{\overline{\text{MS}}}^{(4)} = 319$  MeV [49]. For the

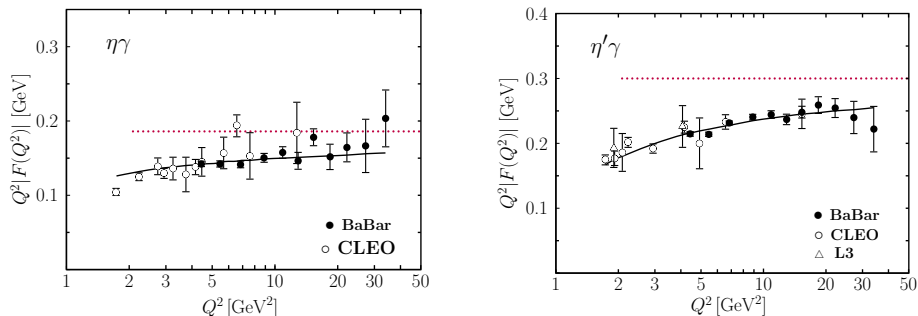


Figure 2: The  $\eta\gamma$  (left) and  $\eta'\gamma$  (right) transition form factors scaled by  $Q^2$ . Data taken from [2, 8, 9]. The solid lines represents our default fit (see Tab. 2). The dotted lines are the LO asymptotic results (28).

factorization and renormalization scales we adopt the frequently used choice  $\mu_F = \mu_R = Q$  which conveniently avoids the  $\ln(Q^2/\mu_F^2)$  terms in (35) and, hence, a contingent resummation of these logarithms [51, 50]. In Sect. 5.1.1 we will comment on other choices for these scales.

Using this standard setting together with the mixing parameters derived in [37], we fit the Gegenbauer coefficients of order 2 to the data <sup>7 8 9</sup> [2, 8]. The result of this fit, termed the default fit in the following, is quoted in Tab. 2 and shown in Fig. 2. For comparison the results of fits to only the CLEO data [8] and only the BaBar data [2] are also shown in Tab. 2. The latter fit can be regarded as a change of the minimal value of  $Q^2$  for which data are taken into account in the fits. One notices that the three sets of parameters for the quark distribution amplitudes agree quite well with each other. Deviations of a little more than  $1\sigma$  are seen for  $a_2^g$ . The effect of the Babar data in combination with the CLEO one results in a reduction of the parameter errors and a more precise determination of  $a_2^g$ . In contrast to our previous work where we have had at disposal only the CLEO data [8] and have chosen  $\mu_R = Q/\sqrt{2}$  and  $\mu_F = Q$ , the gluon distribution amplitude is

<sup>7</sup>The signs of the transition form factors are not measured.

<sup>8</sup>The CLEO collaboration [8] measured the form factors for various  $\eta(\eta')$  decay channels. We take into account all of them. In cases where for a given value of  $Q^2$  there are several values of the form factor we use their error-weighted average.

<sup>9</sup>Above  $Q^2 = 2 \text{ GeV}^2$  there is only one  $\eta'\gamma$  data point from [9] with a large error. It has no bearing on our fits and will therefore not mentioned explicitly in the following.

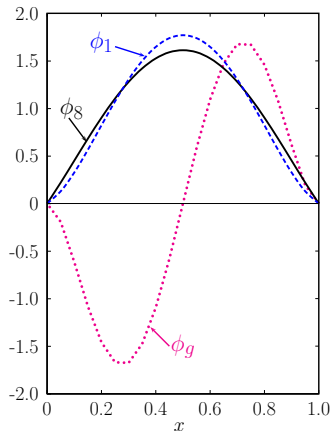


Figure 3: The distribution amplitudes specified by the default fit at the initial scale.

not compatible with zero now. The reasonable agreement of the three fits demonstrates the consistency of the CLEO [8] and BaBar data [2]. The  $\chi^2$  of the default fit is very good given that all together 40 data points are included in the fit. In Fig. 2 the fit is compared to experiment.

The distribution amplitudes corresponding to the default fit (see Tab. 2) are shown in Fig. 3. Those for the octet and singlet  $q\bar{q}$  components are close to the asymptotic form of a meson distribution amplitude. They are symmetric around  $x = 1/2$  while the gluon distribution amplitude is antisymmetric. We repeat that the distribution amplitudes are to be considered as effective ones since the parameters  $a_2$  are contaminated by higher order Gegenbauer coefficients.

### 5.1.1 Scale dependence

Let us discuss the choices of the scales in more detail. In principle, renormalization and factorization scales can be chosen independently. In this work we have chosen  $\mu_R = \mu_F = Q$  for the default fit but we also investigate other choices of the scales in order to learn about the theoretical uncertainties of our results.

First, we discuss our factorization scale choice. As elaborated in [50], the dependence on  $\mu_F$  can be cancelled order by order in  $\alpha_s$  by performing the re-

summation of  $(\alpha_s \ln \mu_F^2/Q^2)^n$  terms<sup>10</sup>, i.e. by performing the evolution of the hard scattering part from  $\mu_F$  to  $Q$  the same way the logs  $(\alpha_s \ln \mu_0^2/\mu_F^2)^n$  are resummed in the distribution amplitude by employing the evolution equation. Occasionally, however, one evolves the distribution amplitude(s) from  $\mu_0$  to  $\mu_F$ , and does not resum the logs in the hard-scattering amplitude, thus causing a residual dependence on  $\mu_F$  even after the convolution with distribution amplitude(s). But the choice  $\mu_F = Q$  corresponds to evolving distribution amplitude(s) all the way from  $\mu_0$  to  $Q$  and removing all  $\ln \mu_F^2/Q^2$  terms from the hard-scattering part. This result is equivalent to evolution of distribution amplitude from  $\mu_0$  to any  $\mu_F$  and the resummation of  $(\alpha_s \ln \mu_F^2/Q^2)^n$  terms in the hard-scattering part and in this sense the choice  $\mu_F = Q$  appears convenient.

For the renormalization scale the usual choice is  $\mu_R = Q$ . On the basis of a next-next-to-leading order calculation of the pion transition form factor it has been argued in [51, 50] that another possible choice of  $\mu_R$  is the square root of the average virtuality instead of the characteristic scale of the process,  $Q$ . For the transition form factors the average virtuality is  $Q^2/2$ . Hence, in order to explore the renormalization scale dependence of the resulting distribution amplitudes we also utilize this choice. As an inspection of Tab. 2 reveals the dependence of the fit on the renormalization scale is rather strong; the change of  $\mu_R$  from  $Q$  to  $Q/\sqrt{2}$  results in substantial change of the parameters although both the fits are of similar quality. Thus, the theoretical uncertainties of our results are larger than indicated by the errors of the fitted Gegenbauer coefficients.

It is important to note that our NLO calculation is in fact the LO calculation in  $\alpha_s$  and it is a well known fact that in order to stabilize the dependence on  $\mu_R$  the NLO QCD corrections i.e., NNLO corrections to the transition form factor, should be included. At NNLO the presence of  $\alpha_s^2 \ln \mu_R^2/Q^2$  terms stabilizes the dependence on  $\mu_R$  and all predictions fall relatively close (see, for example, [52] for discussion on that point). Concerning fits, one would thus expect that the inclusion of NNLO would considerably decrease the variation of the obtained Gegenbauer coefficients with  $\mu_R$ . Without this stabilizing effect of NNLO we are left with the variation illustrated in Tab. 2.

Finally, we test the strength of the residual dependence on the factoriza-

---

<sup>10</sup>The resummation/evolution in the hard-scattering part should be performed from  $\mu_F$  to the characteristic scale of the process which appears in the logs - in our case  $Q$ . One might say that the question then only remains what is the characteristic scale of the particular process but this is more of a problem for the two scale processes.

Scales	$a_2^1 - a_2^g$	$a_2^8 - a_2^1$	$a_2^8 - a_2^g$
$\mu_R^2 = \mu_F^2 = Q^2$	0.371	0.248	0.057
$\mu_R^2 = Q^2/2$	0.607	0.228	0.057
$\mu_R^2 = \mu_F^2 = Q^2/2$	0.760	0.202	0.058

Table 3: Correlation coefficients obtained in the fits to the CLEO [8] and BaBar [2] data for various choices of the scales. Except of the scales the standard setting and the mixing parameters of [37] are used.

tion if the resummation of the  $(\alpha_s \ln \mu_0^2/\mu_F^2)^n$  terms is ignored. In order to do so we perform a fit with the choice  $\mu_R = \mu_F = Q/\sqrt{2}$ . From the results, quoted in Tab. 2, one sees that the fit mildly depends on  $\mu_F$ . The Gegenbauer coefficients  $a_2^8$  and  $a_2^1$  hardly change. For  $a_2^g$  the scale dependence is a bit more pronounced although the values of  $a_2^g$  agree within errors for the two fits with different  $\mu_F$  but the same renormalization scale.

### 5.1.2 Parameter correlations and evolution

Due to their mixing under evolution we expect the strongest correlation between the Gegenbauer coefficients  $a_2^1$  and  $a_2^g$ . Inspection of Fig. 4 reveals that the correlation is particularly strong for the fit to just the CLEO data but becomes milder for the fit to the combined CLEO and BaBar data. This goes parallel with a reduction of the parameter errors. The strength of the correlation between  $a_2^1$  and  $a_2^g$  depends on the chosen factorization and renormalization scales; it is smallest for the standard setting, see Tab. 3 where we compile the correlation coefficients for the three fits to the CLEO and BaBar data. On the other hand, the correlation between  $a_2^1$  and  $a_2^8$  is milder while  $a_2^g$  and  $a_2^8$  are nearly uncorrelated. The origin of the correlation between  $a_2^8$  and the other Gegenbauer coefficients lies in  $\eta - \eta'$  mixing. The form factor  $F_{\eta\gamma}$  is dominated by the octet contribution ( $a_2^8$ ) while  $F_{\eta'\gamma}$  is mainly fed by the singlet one ( $a_2^1, a_2^g$ ).

The evolution of the Gegenbauer coefficients  $a_2^1$  and  $a_2^g$  is shown on the right hand side of Fig. 4. The coefficients decrease relatively fast from the initial scale, up to about 10 GeV<sup>2</sup> and after that the approach to zero is rather slow. This behavior is a consequence of the properties of the logarithm

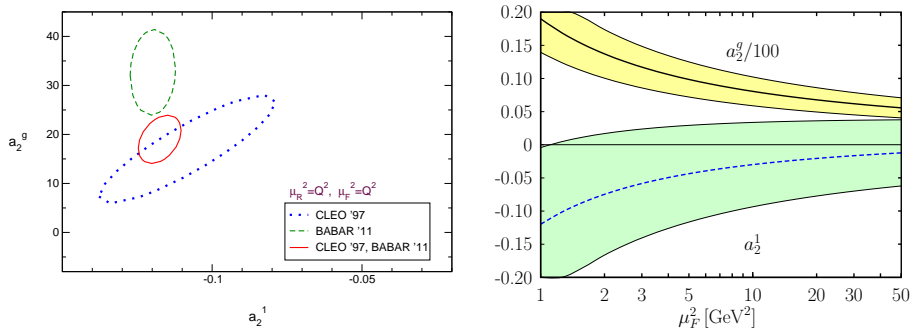


Figure 4: Correlation between  $a_2^1$  and  $a_2^g$  (left) and their evolution (right) for the standard setting. The  $1\sigma$   $\chi^2$ -contours are shown for fits to the data from only CLEO [8], only BaBar [2] and to both data sets. The shaded bands indicate the errors of the coefficients.

contained in  $\alpha_s(\mu_F)$  (see (6)): for  $\mu_F \gg \mu_0$  (in fact for  $\mu_F > 3$  GeV) the derivative of the logarithm is very small. The Gegenbauer coefficients of the octet distribution amplitude evolve similarly. This flat behavior of the logarithm for large scales is also partially responsible for the fact that even in a NLO calculation one can determine only one Gegenbauer coefficient for each distribution amplitude or, more precisely, one linear combination of them.

## 5.2 OZI rule constraints

The valence Fock components of the  $SU(3)_F$  octet-singlet basis can be transformed to those of the quark-flavor basis [6]

$$\begin{aligned}
 |\eta_q\rangle &= \frac{f_q}{2\sqrt{2N_c}} \left[ \phi_q(x, \mu_F) |q\bar{q}\rangle + \phi_{\text{opp}}(x, \mu_F) |s\bar{s}\rangle + \sqrt{\frac{2}{3}} \phi_g(x, \mu_F) |gg\rangle \right] \\
 |\eta_s\rangle &= \frac{f_s}{2\sqrt{2N_c}} \left[ \phi_{\text{opp}}(x, \mu_F) |q\bar{q}\rangle + \phi_s(x, \mu_F) |s\bar{s}\rangle + \frac{1}{\sqrt{3}} \phi_g(x, \mu_F) |gg\rangle \right] \quad (37)
 \end{aligned}$$

where  $q\bar{q}$  is short for the combination  $(u\bar{u} + d\bar{d})/\sqrt{2}$  and

$$\phi_q = \frac{1}{3}(\phi_8 + 2\phi_1), \quad \phi_s = \frac{1}{3}(2\phi_8 + \phi_1), \quad \phi_{\text{opp}} = \frac{\sqrt{2}}{3}(\phi_1 - \phi_8). \quad (38)$$

The new decay constants are related to  $f_8$  and  $f_1$  by

$$f_q = \sqrt{2f_1^2 - f_8^2}, \quad f_s = \sqrt{2f_8^2 - f_1^2}. \quad (39)$$

We see that in (37) the  $s\bar{s}$  ( $q\bar{q}$ ) Fock component appears in the  $\eta_q$  ( $\eta_s$ ) states. These respective opposite Fock components lead to violations of the OZI rule if they were not suppressed. Hence, the consistency of the quark-flavor mixing scheme and the perturbative approach to hard exclusive processes requires that

$$\frac{|\phi_{\text{opp}}(x, \mu_F)|}{\phi_{\text{AS}}(x)} \ll 1 \quad (40)$$

holds for any values of  $x$  at least for a limited range of the factorization scale. Asymptotically, where all distribution amplitudes evolve in  $\phi_{\text{AS}}$ ,  $\phi_{\text{opp}}$  is zero anyway. To a sufficient degree of accuracy (40) can be replaced by

$$\frac{\sqrt{2}}{3} |a_2^1 - a_2^8| \ll 1 \quad (41)$$

Indeed the default fit meets (41) at the initial scale and, as can readily be checked, at all larger factorization scales:  $\frac{\sqrt{2}}{3} |a_2^1 - a_2^8| \lesssim 0.03$ . Hence, no substantial violations of the OZI rule follow from the distribution amplitudes specified by the default fit and shown in Figs. 3. Also the fits using different choices of  $\mu_R$  and  $\mu_F$  as well as those to just the CLEO or BaBar data satisfy (41).

Using the  $\eta - \eta'$  mixing parameters determined in [42] (see Tab. 1) which markedly differ from those given in [37, 38], one also arrives at a reasonable fit to the form factor data with regard to  $\chi^2$ . However, in this case  $a_2^8$  is positive leading to rather large OZI rule violations. The mixing parameters given in [42] are therefore to be employed with reservation. It is to be mentioned that the work [42] has also been criticized in [13] on the basis of an analysis of the transition form factors with a  $U_A(1)$ -anomaly sum rule. The theoretical set of mixing parameters discussed in [41] is intermediate between [37, 38] and [42]. The quality of the fit to the form factor data is similar to other fits but the difference  $|a_2^1 - a_2^8|$  is rather large although smaller than for the fit using the mixing parameters given in [42]. Thus, with regard to the strength of OZI rule violation the mixing parameters given in [37, 38] seem to be favored. Ideally one should fit the mixing parameters together with the lowest Gegenbauer coefficients to the data. Unfortunately such a multi-parameter fit does not lead to a reasonable solution, there are extremely

strong correlations among the parameters, often large violations of the OZI rule and a covariance matrix that is not positive definite. Thus, we refrain from discussing such fits.

In order to avoid large violations of the OZI rule one may follow a suggestion made in [24] and assume  $a_2^1 \equiv a_2^8$  at the initial scale. Although evolution generates some violations of the OZI rule with increasing scale they are always sufficiently small. The fit assuming  $a_2^1 \equiv a_2^8$  and using the mixing parameters of [37, 38] is still of reasonable quality. Although  $\chi^2$  is somewhat larger, the fit parameters are similar to those obtained from the three-parameter fit, see Tab. 2. The difficulties with the OZI rule of the mixing parameters determined in [42] is corroborated by the analogous fit with  $a_2^1(\mu_0) \equiv a_2^8(\mu_0)$ . This fit fails badly,  $\chi^2$  is 240.

### 5.3 Comparison to other results

Ali and Parkhomenko [16] have performed an analysis of the  $\eta'$  energy spectrum in the inclusive decay  $\Upsilon(1S) \rightarrow ggg^* \rightarrow \eta'X$  [53] in order to constrain the  $\eta'$ -meson distribution amplitude. At an intermediate step of the analysis of the  $\Upsilon(1S) \rightarrow \eta'X$  energy spectrum the  $g^* \rightarrow \eta'g$  transition form factor is to be calculated (see Sect. 6). From the high end of the  $\eta'$  meson energy spectrum Ali and Parkhomenko determine the Gegenbauer coefficients  $a_2^1$  and  $a_2^g$  which are in agreement with our results within very large errors. In order to calculate the energy spectrum also at low and even negative gluon virtualities Ali and Parkhomenko introduce a positivity constraint for the  $\eta'g$  transition form factor which is achieved by choosing  $\mu_F^2 = \mu_R^2 = |Q^2| + m_{\eta'}^2$ . This constraint significantly reduce the allowed range for the Gegenbauer coefficients and, in combination with our previous result [6] they obtain

$$a_2^1 = -0.08 \pm 0.03, \quad a_2^g = 6.5 \pm 2.7. \quad (42)$$

at the initial scale  $\mu_0 = 1$  GeV. While the value for  $a_2^1$  agrees with our default result within errors, our result for the coefficient  $a_2^g$  is larger as a consequence of the BaBar data which were not available to the authors of [16]. The role of the positivity constraint used in [16] remains to be understood.

The lowest Gegenbauer coefficient of the octet distribution amplitude has been calculated with the help of QCD sum rules [54]. A value of about 0.2 with a large uncertainty has been obtained for the coefficient  $a_2^8$ . In this calculation the distribution amplitude is normalized to  $f_\eta^8 = f_\pi$ . For the larger

octet decay constant (see Tab. 1) we are using the value of  $a_2^8$  is expected to be somewhat smaller, say, about 0.16. Given the large uncertainty of the sum rule result this value is not in conflict with our default fit. However this large face value of the sum rule result can only be reconciled with the form factor data if one allows for an additional power correction (or for higher Gegenbauer coefficients) which compensate the positive  $a_2^8$  to a large extent. In order to examine this possibility we extract the octet contribution to the transition form factors using (22), (23) and (30)

$$F_{\eta_8\gamma} = \frac{\cos\theta_1 F_{\eta\gamma} + \sin\theta_1 F_{\eta'\gamma}}{\cos(\theta_8 - \theta_1)} \quad (43)$$

and perform a fit analogously to the ones described above but allowing for an additional power correction  $c_8/Q^4$  to it. Keeping  $a_2^8 = 0.16$  fixed and using the mixing parameters determined in [37, 38], we obtain  $c_8 = -0.08 \pm 0.01$  from the fit to the data on  $F_{\eta_8\gamma}$ . For the 15 data points the minimum  $\chi^2$  is 21 which is somewhat larger than our best result ( $\chi^2 = 15.3$  for  $a_2^8 = -0.01 \pm 0.02$ ,  $c_8 = 0$ ) but still tolerable. Freeing also  $a_2^8$  a very good fit is obtained ( $a_2^8 = 0.06 \pm 0.05$ ,  $c_8 = -0.04 \pm 0.02$ ,  $\chi^2 = 16.3$ ). The latter fit is shown in Fig. 5 and compared to experiment. In this figure also the results of the default fit for the octet and singlet form factors

$$F_{\eta_1\gamma} = \frac{\cos\theta_8 F_{\eta'\gamma} - \sin\theta_8 F_{\eta\gamma}}{\cos(\theta_8 - \theta_1)} \quad (44)$$

are displayed and compared with experiment.

## 5.4 A comment on the time-like data

The BaBar collaboration [25] has measured the  $\eta\gamma$  and  $\eta'\gamma$  transition form factors at  $s = 112 \text{ GeV}^2$ . We do not include these data in our analysis since the theoretical treatment of form factors in the time-like region is non-trivial and not well understood. In the time-like region the form factors are no longer real and there are subtleties regarding the analytic continuation from the space- to the time-like region [55] (and references therein).

Compared with the naive expectation that at  $s = 112 \text{ GeV}^2$  the form factor should be close to the asymptotic prediction the Babar result for the  $\eta\gamma$  form factor is about  $2\sigma$  too large. This discrepancy is likely not a consequence of the description of  $\eta - \eta'$  mixing. The quark-flavor mixing scheme is on

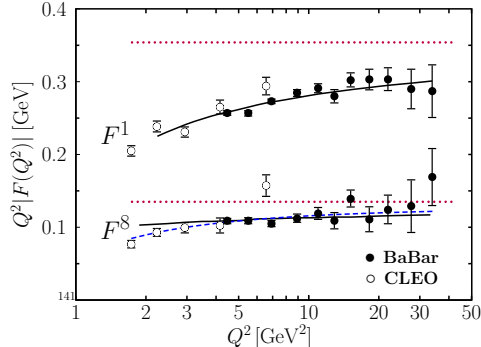


Figure 5: The octet and singlet components of the transition form factors evaluated with the mixing parameters given in [37, 38]. Data taken from [2, 8]. The solid and dotted lines represent our default fit (see Tab. 2) and the asymptotic results, respectively. The dashed line is the fit with a power correction ( $a_2^8 = 0.06 \pm 0.05$ ,  $c_8 = -0.04 \pm 0.02$ ).

sound theoretical grounds and is phenomenologically well established in a large variety of processes. A  $2\sigma$  discrepancy for a single data point cannot discard this mixing scheme. In contrast to the case of the  $\eta$  the  $\eta'\gamma$  form factor at  $s = 112 \text{ GeV}^2$  measured by the BaBar collaboration [25], is in agreement with the naive expectation.

## 6 The $g^*g^*P$ vertex

We are now in the position to repeat the evaluation of the  $g^*g^*P$  form factors we performed in [6]. With the results on the gluon distribution amplitude obtained from the present analysis of the  $P\gamma$  transition form factors we believe to have more precise results for the  $g^*g^*P$  form factors now. On the importance of these form factors we have already commented in the introduction.

The gluonic vertex is written analogously to the electromagnetic one as

$$\Gamma_{ab}^{\mu\nu} = i F_{Pg^*}(\overline{Q}^2, \omega) \delta_{ab} \epsilon^{\mu\nu\alpha\beta} q_{1\alpha} q_{2\beta}, \quad (45)$$

where  $q_1$  and  $q_2$  now denote the momenta of the gluons and  $a$  and  $b$  label the color of the gluon. We consider space-like gluon virtualities for simplicity. It

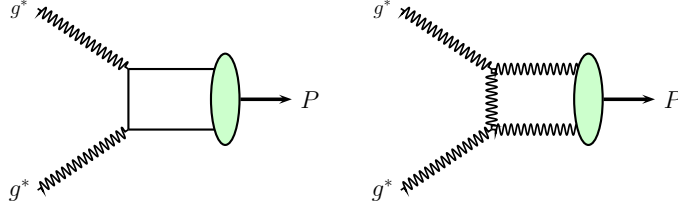


Figure 6: Sample lowest order Feynman graphs for the  $g^*g^* \rightarrow q\bar{q}$  and  $g^*g^* \rightarrow gg$  subprocesses to the  $g^*g^* \rightarrow P$  transition form factors.

is convenient to introduce an average virtuality and an asymmetry parameter:

$$\bar{Q}^2 = -\frac{1}{2}(q_1^2 + q_2^2), \quad \omega = \frac{q_1^2 - q_2^2}{q_1^2 + q_2^2}. \quad (46)$$

The values of  $\omega$  range from  $-1$  to  $1$ , but, due to Bose symmetry, the transition form factor is symmetric in this variable:  $F_{Pg^*}(\bar{Q}^2, \omega) = F_{Pg^*}(\bar{Q}^2, -\omega)$ .

According to [6] the  $Pg^*$  transition form factor to leading-twist accuracy and lowest order of  $\alpha_s$  is to be calculated from Feynman graphs of which examples are shown in Fig. 6. It reads

$$F_{Pg^*}(\bar{Q}^2, \omega) = 4\pi\alpha_s(\mu_R) \frac{f_P^1}{\bar{Q}^2} \frac{\sqrt{N_f}}{N_c} \left[ A_{q\bar{q}}(\omega) + \frac{N_c}{2N_f} A_{gg}(\omega) \right] + \mathcal{O}(\alpha_s^2), \quad (47)$$

where

$$\begin{aligned} A_{q\bar{q}}(\omega) &= \int_0^1 dx \phi_1(x, \mu_F^2) \frac{1}{1 - \omega^2(1 - 2x)^2}, \\ A_{gg}(\omega) &= \int_0^1 dx \frac{\phi_g(x, \mu_F^2)}{x\bar{x}} \frac{1 - 2x}{1 - \omega^2(1 - 2x)^2}. \end{aligned} \quad (48)$$

There are a few more LO Feynman graphs involving triple or quadruple gluon vertices. However, they do not contribute when contracted with the  $q\bar{q}$  or  $gg$  projectors, (11) and (13). The integrals in (48) can be worked out by inserting the Gegenbauer expansions (5) into it and performing the integrals term by term analytically analogously to (35). The results are given in [6] and are not repeated here. Using the Gegenbauer coefficients of the default fit, we can readily evaluate the  $g^*g^* \rightarrow \eta'$  transition form factor. The results, including the  $1\sigma$  error band, are shown in Fig. 7 for two values of  $\bar{Q}^2 = \mu_R^2 = \mu_F^2$ . As

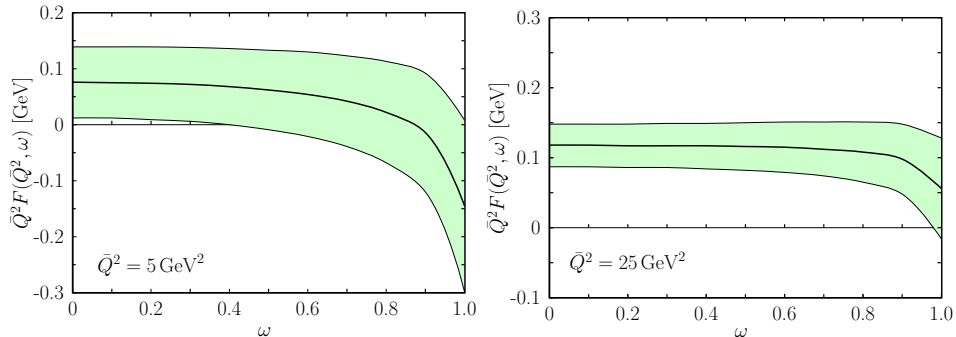


Figure 7: Predictions for the  $g^*g^*\eta'$  form factor evaluated from the default solution with  $\mu_R^2 = \mu_F^2 = \bar{Q}^2$ . The shaded bands indicate the  $1\sigma$  uncertainty of the predictions.

compared to our previous results [6] the error bands are markedly narrower while the central values do not differ much.

The ratio of the  $\eta g^*$  and  $\eta' g^*$  form factors is given by

$$F_{\eta g^*}/F_{\eta' g^*} = f_{\eta}^1/f_{\eta'}^1 = -\tan\theta_1. \quad (49)$$

As for the  $\eta\gamma$  and  $\eta'\gamma$  transition form factors and in order to be consistent with that analysis power corrections are neglected here as well. For the  $g^*g^*\eta(\eta')$  vertex function, in particular for  $\omega \rightarrow 0$ , any power corrections as for instance quark transverse momenta or meson mass corrections, are small since the vertex function is not end-point sensitive in this kinematic limit. Mass corrections to the  $g^*g^*\eta'$  vertex function have been estimated by Ali and Parkhomenko [16, 17].

## 7 The $\pi\gamma$ transition form factor

For comparison we show in Fig. 8 the data on the  $\pi\gamma$  transition form factor [2, 4, 8]. It is important to realize the dramatic difference between the BaBar data [2] on the  $\pi\gamma$  form factor and the  $\eta(\eta')\gamma$  data. In contrast to the latter a leading-twist analysis of the  $\pi\gamma$  form factor to fixed order of perturbative QCD fails because the data do not seem to respect dimensional scaling. Power corrections seem to be demanded by the  $\pi\gamma$  data as well as a positive value of the 2nd Gegenbauer coefficient of the pion distribution amplitude,

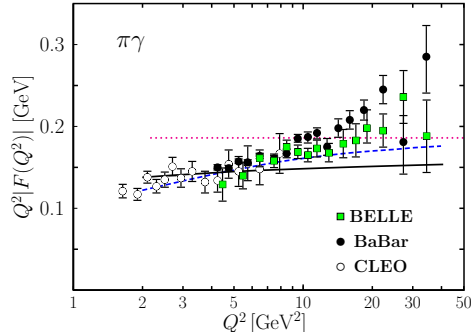


Figure 8: The  $\pi\gamma$  transition form factor. Data taken from [2, 4, 8]. The solid (dashed, dotted) line represents a fit with  $a_2^\pi(\mu_0) = -0.02$  ([29], LO asymptotic result).

see for instance [10, 14, 36]. This difference between the  $\pi\gamma$  and the other form factors implies a strong breaking of flavor symmetry which has never been observed in the sector of pseudoscalar mesons before.

On the other hand, the BELLE data [4] do not show this sharp rise with  $Q^2$ , they lie systematically below the BaBar data. They do not exceed the asymptotic result for the  $\pi\gamma$  form factor and are close to the behavior of the NLO leading-twist approach as is the case of the other transition form factors. An example of such a fit to the data from [8] and [4] is shown in Fig. 8 (with  $a_2^\pi(\mu_0) = -0.02 \pm 0.02$  and  $\chi^2 = 34.9$  for 28 data points). Although the  $\chi^2$  of this fit is reasonable the  $Q^2$  dependence of the fit seems to be too flat as compared to the BELLE data which may be viewed as a hint at lacking power corrections. For instance, a result obtained with  $k_\perp$  factorization which encodes corrections of order  $\langle k_\perp^2/Q^2 \rangle$ , is in good agreement with the CLEO and BELLE data [29]. We finally emphasize that the BELLE data imply only mild violations of flavor symmetry. A more detailed comparison of the BaBar and BELLE data with theoretical models can be found in [60]. Although the BELLE data seem to be favored against the BaBar data with regard to the standard theoretical concepts, an understanding of the origin of the discrepancy between the two measurements is required.

## 8 Summary

We have analyzed the  $\eta\gamma$  and  $\eta'\gamma$  transition form factors within a collinear factorization approach to leading-twist accuracy and NLO of perturbative QCD. The analysis of the data [2, 8] allowed for an extraction of the lowest Gegenbauer coefficients of the  $q\bar{q}$  flavor-octet and singlet distribution amplitudes as well as that of the glue-gluon distribution amplitude. The Gegenbauer coefficients are better determined now and have smaller errors than those extracted in [6]. Our default result for  $\mu_0 = 1$  GeV is (see Tab. 2):

$$a_2^8 = -0.05 \pm 0.02, \quad a_2^1 = -0.12 \pm 0.01, \quad a_2^g = 19 \pm 5. \quad (50)$$

There are a number of uncertainties of this result. First there is the uncertainty due to the chosen renormalization scale. Next, despite the large range of  $Q^2$  covered by data now one still cannot determine more than the lowest Gegenbauer coefficients of the three distribution amplitudes. The coefficients we quote are to be regarded as effective parameters which are contaminated by higher order Gegenbauer coefficients. In fact, according to the discussion at the end of Sect. 5.1.2, it seems impossible to extract more information from the transition form factors than the lowest Gegenbauer coefficients. In order to determine more Gegenbauer coefficients additional processes have to be analyzed. Finally, given the quality of the present data, it is still not possible to discriminate between the logarithmic  $Q^2$  dependence generated by the evolution and the NLO corrections, and power corrections (see the discussion in Sect. 5.3). We have neglected power correction in our analysis. Allowing for power corrections in the form factor analysis one may for instance find positive  $q\bar{q}$  Gegenbauer coefficients as is the case for the pion distribution amplitude (e.g. [36]).

As an application of our results for the Gegenbauer coefficients we calculated the  $g^*g^*\eta'$  vertex function. Another processes in which the gluon-gluon Fock components of the  $\eta$  and  $\eta'$  mesons may play an important role, are the  $\chi_{cJ}$  ( $J = 0, 2$ ) decays into pairs of  $\eta$  and/or  $\eta'$  mesons. Here, the  $c$ -quark mass is considered to be large enough to allow for a perturbative treatment of these decays. An explicit calculation of the perturbative contribution to the  $\chi_{cJ}$  decays taking into account the two-gluon Fock components, is tedious, many Feynman graphs contribute even to lowest order [56]. Moreover, there is another complication. As is shown in [57] the next higher Fock state,  $c\bar{c}g$ , of the  $\chi_{cJ}$ , the so-called color-octet contribution [58], is also to be taken into account since it scales with the same power of the hard scale,  $m_c$ , as

the  $c\bar{c}$  contribution. With regard to these complications whose detailed calculation is very time-consuming, we will not attempt a complete analysis of these decay processes; this is beyond the scope of the present paper. A statement whether or not our  $gg$  distribution amplitudes are in conflict with the peculiar features of the  $\chi_{cJ}$  decays [46, 49, 59] is therefore premature.

This work was supported in part by the BMBF under the contract No. 06RY9191 and in part by Croatian Ministry of Science, Education and Sport under the contract no. 098-0982930-2864.

## References

- [1] B. Aubert *et al.* [The BABAR Collaboration], Phys. Rev. D **80**, 052002 (2009) [arXiv:0905.4778 [hep-ex]].
- [2] P. del Amo Sanchez *et al.* [BABAR Collaboration], Phys. Rev. D **84**, 052001 (2011) [arXiv:1101.1142 [hep-ex]].
- [3] G. P. Lepage and S. J. Brodsky, Phys. Lett. B **87**, 359 (1979).
- [4] S. Uehara *et al.* [Belle Collaboration], arXiv:1205.3249 [hep-ex].
- [5] T. Feldmann and P. Kroll, Eur. Phys. J. C **5**, 327 (1998) [hep-ph/9711231].
- [6] P. Kroll, K. Passek-Kumericki, Phys. Rev. **D67**, 054017 (2003). [hep-ph/0210045].
- [7] S. S. Agaev, N. G. Stefanis, Phys. Rev. **D70**, 054020 (2004). [hep-ph/0307087].
- [8] J. Gronberg *et al.* [CLEO Collaboration], Phys. Rev. D **57**, 33 (1998) [hep-ex/9707031].
- [9] M. Acciarri *et al.* [L3 Collaboration], Phys. Lett. B **418**, 399 (1998).
- [10] P. Kroll, Eur. Phys. J. **C71**, 1623 (2011). [arXiv:1012.3542 [hep-ph]].
- [11] S. J. Brodsky, F. -G. Cao, G. F. de Teramond, Phys. Rev. D **84**, 075012 (2011) [arXiv:1105.3999 [hep-ph]].

- [12] A. E. Dorokhov, A. E. Radzhabov, A. S. Zhevlakov, Eur. Phys. J. C **71**, 1702 (2011) [arXiv:1103.2042 [hep-ph]].
- [13] Y. N. Klopot, A. G. Oganesian, O. V. Teryaev, Phys. Rev. D **84**, 051901 (2011) [arXiv:1106.3855 [hep-ph]].
- [14] D. Melikhov and B. Stech, arXiv:1202.4471 [hep-ph].
- [15] S. Noguera and S. Scopetta, arXiv:1110.6402 [hep-ph].
- [16] A. Ali, A. Y. Parkhomenko, Eur. Phys. J. **C30**, 183 (2003). [hep-ph/0304278].
- [17] A. Ali, A. Y. Parkhomenko, Eur. Phys. J. **C30**, 367-380 (2003). [arXiv:hep-ph/0307092 [hep-ph]].
- [18] L. A. Harland-Lang, V. A. Khoze, M. G. Ryskin, W. J. Stirling, Eur. Phys. J. C **71**, 1714 (2011) [arXiv:1105.1626 [hep-ph]].
- [19] M. Gronau and J. L. Rosner, Phys. Rev. D **53**, 2516 (1996)
- [20] M. Beneke, M. Neubert, Nucl. Phys. **B675**, 333-415 (2003). [hep-ph/0308039].
- [21] A. R. Williamson, J. Zupan, Phys. Rev. **D74**, 014003 (2006). [hep-ph/0601214].
- [22] J. Schumann *et al.* [ Belle Collaboration ], Phys. Rev. Lett. **97**, 061802 (2006). [hep-ex/0603001].
- [23] B. Aubert *et al.* [ The BABAR Collaboration ], Phys. Rev. **D80**, 112002 (2009). [arXiv:0907.1743 [hep-ex]].
- [24] P. Ball, G. W. Jones, JHEP **0708**, 025 (2007). [arXiv:0706.3628 [hep-ph]].
- [25] B. Aubert *et al.* [BABAR Collaboration], Phys. Rev. D **74**, 012002 (2006) [hep-ex/0605018].
- [26] M. V. Terentev, Sov. J. Nucl. Phys. **33**, 911 (1981) [Yad. Fiz. **33**, 1692 (1981)].
- [27] V. N. Baier and A. G. Grozin, Nucl. Phys. B **192**, 476 (1981).

- [28] D. Müller, Phys. Rev. D **51**, 3855 (1995) [hep-ph/9411338].
- [29] P. Kroll and M. Raulfs, Phys. Lett. B **387**, 848 (1996) [hep-ph/9605264].
- [30] G. P. Lepage and S. J. Brodsky, Phys. Rev. D **22**, 2157 (1980).
- [31] J. B. Kogut and D. E. Soper, Phys. Rev. D **1**, 2901 (1970).
- [32] R. Kaiser and H. Leutwyler, Eur. Phys. J. C **17**, 623 (2000) [hep-ph/0007101].
- [33] A. V. Belitsky and D. Mueller, Nucl. Phys. B **537**, 397 (1999) [hep-ph/9804379].
- [34] F. del Aguila and M. K. Chase, Nucl. Phys. B **193**, 517 (1981);
- [35] E. Braaten, Phys. Rev. D **28**, 524 (1983);
- [36] S. S. Agaev, V. M. Braun, N. Offen, F. A. Porkert, Phys. Rev. **D83**, 054020 (2011). [arXiv:1012.4671 [hep-ph]].
- [37] T. Feldmann, P. Kroll, B. Stech, Phys. Rev. **D58**, 114006 (1998). [hep-ph/9802409].
- [38] T. Feldmann, P. Kroll, B. Stech, Phys. Lett. **B449**, 339-346 (1999). [hep-ph/9812269].
- [39] F. De Fazio, M. R. Pennington, JHEP **0007**, 051 (2000). [hep-ph/0006007].
- [40] E. B. Gregory, A. C. Irving, C. M. Richards and C. MacNeile [UKQCD collaboration], arXiv: 1112.4384 [hep-lat].
- [41] P. Kroll, Mod. Phys. Lett. **A20**, 2667-2684 (2005). [hep-ph/0509031].
- [42] R. Escribano, J. -M. Frere, JHEP **0506**, 029 (2005). [hep-ph/0501072].
- [43] J. L. Goity, A. M. Bernstein, B. R. Holstein, Phys. Rev. **D66**, 076014 (2002). [hep-ph/0206007].
- [44] J. Schechter, A. Subbaraman, H. Weigel, Phys. Rev. **D48**, 339-355 (1993). [hep-ph/9211239].

- [45] C. Di Donato, G. Ricciardi, I. Bigi, Phys. Rev. D **85**, 013016 (2012) [arXiv:1105.3557 [hep-ph]].
- [46] C. E. Thomas, JHEP **0710**, 026 (2007). [arXiv:0705.1500 [hep-ph]].
- [47] V. Crede, C. A. Meyer, Prog. Part. Nucl. Phys. **63**, 74-116 (2009). [arXiv:0812.0600 [hep-ex]].
- [48] M. Diehl, P. Kroll, C. Vogt, Eur. Phys. J. **C22**, 439-450 (2001). [hep-ph/0108220].
- [49] K. Nakamura *et al.* [ Particle Data Group Collaboration ], J. Phys. G **G37**, 075021 (2010).
- [50] B. Melić, B. Nižić and K. Passek, Eur. Phys. J. C **36**, 453 (2004) [arXiv:hep-ph/0107311 [hep-ph]].
- [51] B. Melić, B. Nižić and K. Passek, Phys. Rev. D **65**, 053020 (2002) [hep-ph/0107295].
- [52] B. Melić, B. Nižić and K. Passek, Phys. Rev. D **60**, 074004 (1999) [hep-ph/9802204].
- [53] M. Artuso *et al.* [CLEO Collaboration], Phys. Rev. D **67**, 052003 (2003) [hep-ex/0211029].
- [54] P. Ball, JHEP **9901**, 010 (1999). [hep-ph/9812375].
- [55] A. P. Bakulev, A. V. Radyushkin and N. G. Stefanis, Phys. Rev. D **62**, 113001 (2000) [hep-ph/0005085].
- [56] V.N. Baier and A.G. Grozin, Z. Phys. **C29**, 161 (1985).
- [57] J. Bolz, P. Kroll and G. A. Schuler, Eur. Phys. J. C **2**, 705 (1998) [hep-ph/9704378].
- [58] G. T. Bodwin, E. Braaten and G. P. Lepage, Phys. Rev. D **51** (1995) 1125.
- [59] H. -B. Li [ BESIII Collaboration ], PoS **FPCP2010**, 004 (2010). [arXiv:1101.2049 [hep-ex]].
- [60] A. P. Bakulev, S. V. Mikhailov, A. V. Pimikov and N. G. Stefanis, arXiv:1205.3770 [hep-ph].